Hindawi Publishing Corporation
Journal of Nanomaterials
Volume 2013, Article ID 561534, 7 pages
http://dx.doi.org/10.1155/2013/561534

Research Article

Influence of TiO_2 Nanoparticles on Enhancement of Optoelectronic Properties of PFO-Based Light Emitting Diode

Bandar Ali Al-Asbahi,[1,2] Mohammad Hafizuddin Haji Jumali,[1] Chi Chin Yap,[1] and Muhamad Mat Salleh[3]

[1] *School of Applied Physics, Faculty of Science and Technology, Universiti Kebangsaan Malaysia (UKM), 43600 Bangi, Selangor, Malaysia*
[2] *Department of Physics, Faculty of Science, Sana'a University, Sana'a, Yemen*
[3] *Institute of Microengineering and Nanoelectronics (IMEN), Universiti Kebangsaan Malaysia (UKM), 43600 Bangi, Selangor, Malaysia*

Correspondence should be addressed to Bandar Ali Al-Asbahi; alasbahibandar@gmail.com and Mohammad Hafizuddin Haji Jumali; hafizhj@ukm.my

Received 4 July 2013; Revised 25 September 2013; Accepted 25 September 2013

Academic Editor: Yanbao Zhao

Improvement on optoelectronic properties of poly (9,9′-di-n-octylfluorenyl-2.7-diyl)- (PFO-) based light emitting diode upon incorporation of TiO_2 nanoparticles (NPs) is demonstrated. The PFO/TiO_2 nanocomposites with different weight ratios between 5 and 35 wt.% were prepared using solution blending method before they were spin coated onto Indium Tin Oxide substrate. Then a thin Al layer was deposited onto the nanocomposite layer to act as top electrode. The nanocomposites were tested as emissive layer in organic light emitting diodes (OLEDs). The TiO_2 NPs played the most crucial role in facilitating charge transport and electrical injection and thus improved device performance in terms of turn-on voltage, electroluminescence spectra (EL), luminance, and luminance efficiency. The best composition was OLED with 5 wt.% TiO_2 NPs content having moderate surface roughness and well distribution of NPs. The device performance was reduced at higher TiO_2 NPs content due to higher surface roughness and agglomeration of TiO_2 NPs. This work demonstrated the importance of optimum TiO_2 NPs content with uniform distribution and controlled surface roughness of the emissive layer for better device performance.

1. Introduction

Organic light emitting diodes (OLEDs) are relatively more efficient compared to inorganic light emitting diodes since they require a relatively small amount of power for the same amount of light produced. Besides that, OLEDs offer several merits such as easy to fabricate, low cost, flexible, and low operating voltage. Typical polymers used in organic light emitting diodes (OLEDs) displays include derivatives of poly (*p*-phenylene vinylene) (PPV) and polyfluorene (PF). Regrettably, PPV and PF-based light emitting diodes performance are limited by their poor stability as well as low luminance efficiency. The main reason for the low luminance efficiency is low electron mobility, and high energy barrier between the emissive layer and the electrodes resulted in poor electron injection. Incorporation of inorganic semiconductor, which have low energy barrier to electron injection and high electron mobility into polymer, is one way to resolve the transport and electron injection limitations [1–5].

In recent years, polymer/inorganic nanocomposites received much attention from a great number of researchers [6–8]. This is because the composite systems were reported to exhibit better thermal, mechanical, optical, and electrical properties in comparison to the pure polymer. Earlier studies suggested that the suitability and compatibility of any nanocomposite materials for optoelectronic applications can be predicted from detailed study on their fundamental properties in particular conjugated length, energy gap, and energy transfer efficiency [9, 10]. Recently we predicted the suitability of poly (9,9′-di-n-octylfluorenyl-2.7-diyl) (PFO)/TiO_2 nanocomposite as an emissive layer in OLED devices [11].

The PFO has highest occupied molecular orbital (HOMO) of −5.9 eV and lowest unoccupied molecular orbital (LUMO) of −2.9 eV [12], while the work function values of Indium Tin Oxide (ITO) and Al electrodes are −4.8 eV and −4.3 eV, respectively [13]. Based on these values, the barrier height between the HOMO of PFO and the ITO is much smaller than the barrier height between the LUMO of PFO and the Al electrode (Figure 1). Together with poor electron mobility compared to hole mobility in PFO, huge barrier height between the LUMO of PFO and the Al electrode resulted in the notorious charge imbalance problem in PFO. Insertion of suitable entity into PFO matrix to form a small barrier height for electron injection is thought as the best solution for this problem.

This work investigated the effect of TiO_2 NPs contents (valence band and conduction band of −7.4 eV and −4.2 eV, resp. [14]) embedded into PFO on the formation of a smaller barrier height for electron injection at PFO/Al interface. In addition, this work reports the effect of TiO_2 NPs content on performance of the PFO-based OLED in terms of turn-on voltage, electroluminescence spectra (EL), luminance, and luminance efficiency. The Commision International de I'Eclairage (CIE) chromaticity diagram was used to map the colors of the OLED devices. Finally, the effect of the film morphology on the device performance was demonstrated.

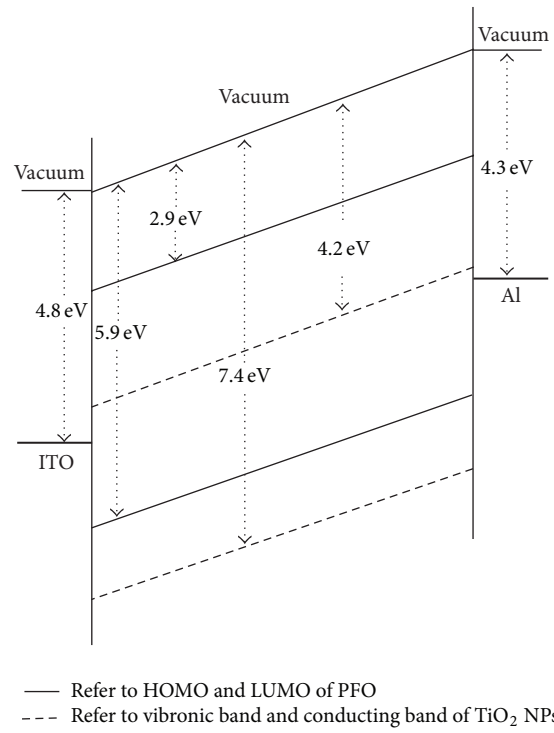

Figure 1: Energy band diagram for Al/PFO:TiO_2/ITO OLED device relative to vacuum.

2. Experimental Procedures

2.1. Materials. The poly (9,9′-di-n-octylfluorenyl-2.7-diyl) (PFO) (M_w = 58200) and TiO_2 powder (mean size of 25 nm) were purchased from Sigma Aldrich, USA. These materials were stored in the dry box and used without further purification. All materials were dissolved in toluene solvent produced by Fluka. ITO coated glass substrate with a sheet resistance of 50 Ω/sq was purchased from Merck Balzers and used in this study.

2.2. Samples Preparation and OLED Fabrication. As previously reported [11], the solution blending method was employed for the preparation of PFO/TiO_2 nanocomposites. TiO_2 NPs with different weight ratios (5, 15, 25, and 35 wt.%) were added into fixed concentration of PFO (15 mg/mL). The mixtures were stirred at 600 rpm overnight followed by sonication for 1 h to get homogeneous nanocomposite solutions.

Prior to OLED fabrications, the ITO which served as anode was firstly etched and patterned by exposing to the vapor of nitric acid (HNO_3) and hydrochloric acid (HCl) in a molar ratio of 3 : 1. Next, the ITO was cleaned sequentially in isopropanol and acetone under ultrasonication for 10 minutes each to clean the surface and remove any impurities.

Using spin coating technique, 100 μL of PFO/TiO_2 nanocomposite solution was deposited onto a substrate with dimensions of 1.2 cm × 2 cm to form a thin layer. The deposition parameters were fixed at 2000 rpm for 30 sec. Then, it was baked at 120°C for 10 minutes in a vacuum oven to remove the solvent from the film. A thin aluminum layer on the nanocomposite film was deposited using electron beam chamber with deposition rate of 2 Å/min at the chamber pressure of 2.5 × 10^{-6} Pa.

2.3. Samples Characterization. The current density-voltage (J-V) was obtained using a Keithley 238 measurement system, whereas electroluminescence spectra (EL), luminance, and color measurements were obtained using HR2000 Ocean Optic Spectrometer. The values of turn-on voltage for all devices are defined as the voltage at the device luminance of 0.5 cd/m^2. The surface morphology of the films was investigated by Scanning Probe Microscope (SPM) in tapping mode using phosphorous doped Si probe (model Veeco CONT20A-CP, part no. MPP-31123-10).

3. Results and Discussion

3.1. Current Density-Voltage Measurements. The current density-voltage (J-V) characteristics of the pristine PFO and PFO/TiO_2 nanocomposites OLED devices are shown in Figure 2. Continuous reduction in turn-on voltage of injection current was observed in the PFO/TiO_2 nanocomposite devices as compared to the pure PFO (Table 1). These positive findings can be understood as better injection of charge carrier resulted from lower potential barrier at the nanocomposite-electrode interface [15]. On the other hand, the rising of current density with the TiO_2 NPs content may possibly attributed to reduction in both the resistance and activation energy of the PFO/TiO_2 layer which facilitated charge transport [1, 12].

Table 1: Optoelectronic characteristics of pristine PFO and PFO/TiO_2 nanocomposite light-emitting diodes at various contents of the TiO_2 NPs.

Emissive layer	Max. luminance (cd/m^2)	Luminance efficiency[a] (cd/A)	Turn-on voltage[b] (V)	CIE coordinates[a]		Current density[a] (mA/cm^2)
				X	Y	
Pristine PFO	30 at 31 V	0.044	18	0.332	0.486	68.6
5 wt.% TiO_2	252 at 29 V	0.11	16	0.347	0.489	220.0
15 wt.% TiO_2	232 at 25 V	0.06	14	0.373	0.500	373.2
25 wt.% TiO_2	117 at 18 V	0.02	11	0.374	0.509	589.0
35 wt.% TiO_2	7 at 16 V	0.0004	13	0.375	0.477	1783.6

[a]At maximum luminance, [b]at luminance of 0.5 cd/m^2 as standard.

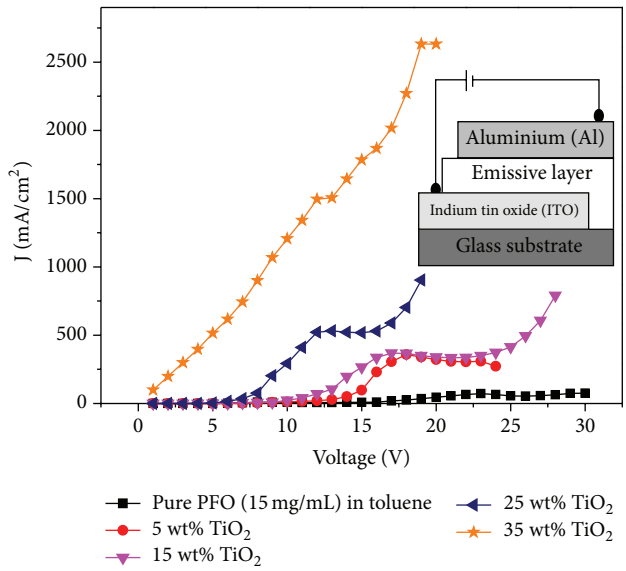

Figure 2: Current density-voltage (J-V) characteristic of the PFO and PFO/TiO_2 OLED devices. The insert shows the schematic diagram of OLED.

However, once the TiO_2 NPs content increased to 35 wt.%, the J-V curve displayed almost a linear relationship, indicating a change in electrical behavior from semiconductor to resistor behavior. It was found later that this behavior was influenced by its surface profile as evidence from SPM images (Section 3.5).

3.2. Electroluminescence Spectra. The electroluminescence (EL) spectra of pristine PFO and PFO/TiO_2 nanocomposite films, under forward bias and at the maximum luminescence, are compared in Figure 3. It can be seen that all devices yielded a broad EL spectra.

The PFO device was observed to emit photons at 428, 450, and 525 nm (Figure 3). The first two blue peaks were consistent with the PFO, which correspond to photoluminescence spectra (PL) [11]. These peaks are attributed to the excitonic emission and its vibronic progression from noninteracting single chains [16]. The third peak is due to the formation of fluorenone defects (keto defects) which are incorporated as C=O in the PFO backbone [17–19]. The photooxidation, electrooxidation, and thermal oxidation are the major reasons for the generation of fluorenone ($(C_6H_4)_2C=O$) defect, which created lower energy emission at 525 nm. Since such defects are mainly generated during fabrication of the device, the low energy emission band (525 nm) is typically more intense in EL than PL.

In the case of PFO/TiO_2 nanocomposite devices, the same EL peaks of the PFO were observed, where the emission band (from 525 to 700 nm) was extended with the TiO_2 NPs increment. Similar trend was reported earlier in PFO/ZnO LED [2]. It is believed that this extended emission band was due to the presence of different defect sources in the materials such as oxygen vacancies (V_O), metal ion vacancies (V_{Ti}), or recombination of electrons with surface states in metal oxides.

Additionally, all composite devices (up to 25 wt.% TiO_2 NPs) exhibited better EL intensity compared to that of pristine PFO. Among these devices, it is clearly observed that the device with 5 wt.% of TiO_2 NPs has the highest EL intensity which is attributed to the best balancing between holes and electrons and thus highest electrons-holes recombination [20]. However, device with 35 wt.% TiO_2 NPs displayed inferior optoelectronic properties compared to all devices, as will be interpreted in Sections 3.3 and 3.5.

3.3. Luminance (cd/cm^2) and Luminance Efficiency (cd/A). There are two crucial factors for an enhancement of both luminance and luminance efficiency upon inclusion of the TiO_2 NPs into the PFO. The first is the decrease of LUMO barrier height at electrode interface (Figure 1). The second factor is higher electron mobility in TiO_2 NPs (1.7×10^{-4} cm^2/Vs) [21] compared to that of hole in PFO (1.6×10^{-5} cm^2/Vs) [17], which lead to recombination of both electron and hole took place in the PFO.

Figure 4 displays the luminance-voltage characteristics of the PFO and PFO/TiO_2 OLED devices. It was confirmed that the device luminance was improved with increasing the TiO_2 NPs content. As an example, the maximum luminance was enhanced from 30 cd/m^2 at current density of 68.6 mA/cm^2 in pristine PFO device to 252 cd/m^2 at current density of 220 mA/cm^2 in the PFO/TiO_2 device with 5 wt.% TiO_2 NPs. Similar positive trend was observed for luminance efficiency. This means that the incorporation of the TiO_2 NPs enhanced

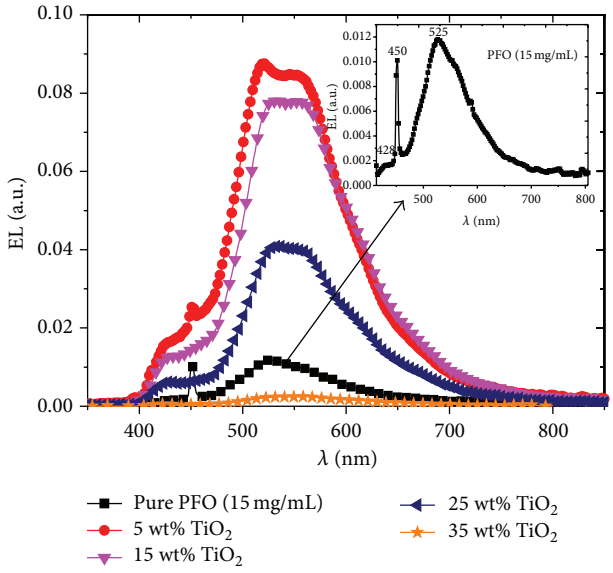

Figure 3: EL spectra of PFO and PFO/TiO_2 devices with different content of TiO_2 NPs and at applied voltages corresponding to maximum luminance.

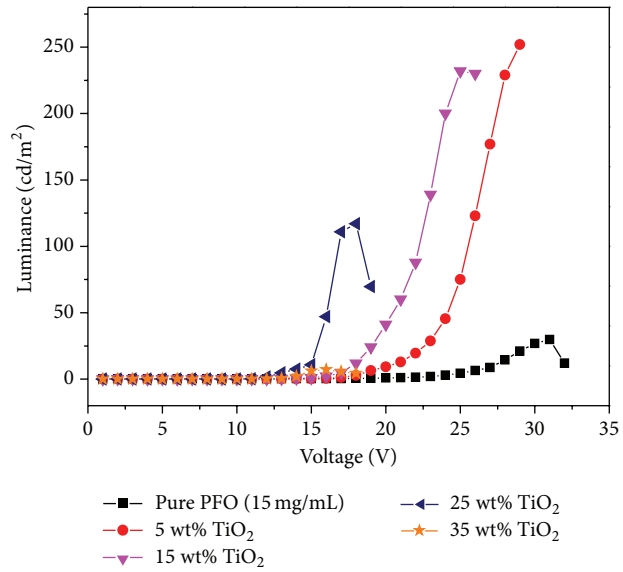

Figure 4: Luminance-voltage characteristics for PFO with various weight ratios of TiO_2 NPs.

the luminance, luminance efficiency, and current density of the PFO device between 250% and 800%. This dramatic enhancement was attributed to the incorporation of the TiO_2 NPs which decreased the LUMO barrier height from 1.4 eV for PFO to 0.1 eV at the PFO/Al interface as shown in Figure 1. In addition, at the PFO/TiO_2 interface, the high potential barrier of electron injection (1.4 eV) leads to entrapment of the electrons in the PFO side, before recombination with incoming holes from the ITO (anode) resulted in high luminance. The suggested mechanism of these processes is presented in Figure 5(a). It is worth noting that the hole-electron recombination in the TiO_2 side is not allowed, which was evidenced by absence of any peaks in the ultraviolet region as shown in EL spectra (Figure 3).

Dramatic reduction of luminance and EL intensity was recorded once the TiO_2 NPs content exceeded 25 wt.%. This could be due to either electrons hopping into the conduction band of the TiO_2 or the electrons tunnel through the emissive layer of the PFO without recombining with the holes or combination of both as illustrated in Figure 5(b). This electron hopping and tunneling became severe when there is poor distribution of nanoparticles on the emissive layer.

3.4. Color Measurements. Figure 6 shows the typical CIE coordinates of PFO/5 wt.% TiO_2 OLED device when the applied voltage was increased from 18 to 29 V. The consistency between CIE coordinates and the analysis of EL spectra was clearly observed. This figure displays that a shift was demonstrated with a rise in the applied voltage. The CIE coordinates were red-shifted from (0.319, 0.487) to (0.346, 0.505) upon rising applied voltage from 18 to 26 V. After that, it shifted from (0.346, 0.503) to (0.347, 0.489) as the applied voltage increased from 27 to 29 V.

As summarized in Table 1, a slight shift in CIE coordinate was demonstrated with the rise of the TiO_2 NPs content at the applied voltage which caused maximum luminance. This means that the produced color was stable, which was consistent with EL spectra (Figure 3). As the applied voltage increased, more electrons could be transported across the PFO/TiO_2 high energy barrier into the LUMO of PFO and thus the exciton recombination in the PFO side was increased. On the other hand, the CIE coordinates variation when the applied voltage increased could be attributed to the rise in sensitivity of the electric field during the carrier transport and injection [22]. The increase in the electric field on both boundaries of the emitting layer was caused by the relatively high voltage. Moreover, the red-shift in CIE coordinates as the applied voltage increase is attributed to the extension of the recombination zone as well as keto-type defect formation [22].

3.5. Morphology of PFO/TiO_2 Nanocomposite Films. Surface morphology of pristine PFO and PFO/TiO_2 films in OLED were observed to play a crucial role in device performance. Figure 7 shows SPM micrographs of PFO and PFO/TiO_2 films, which were measured over an area of $2.5 \times 2.5\,\mu m^2$. Large protuberance formed on the surface of the PFO/TiO_2 nanocomposite films as compared to pristine PFO film. Formation of large protuberance was attributed to the agglomeration of TiO_2 NPs due to strong electrostatic force during the deposition process [23]. This observation was in good agreement with the previous report [11].

The root mean square (RMS) roughness exhibited dramatic increment from 1.402 to 77.80 nm as shown in Figure 8. During deposition, the PFO was liquid wetted in the TiO_2 NPs in an effect known as capillarity which consequently increased the surface roughness. This induced roughness at

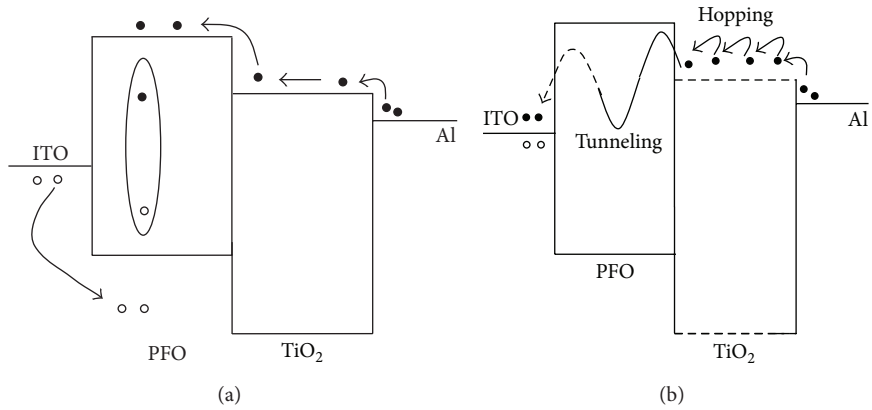

Figure 5: Mechanism of (a) charge injection/transport and (b) hopping and tunneling of electrons in the OLED device. (Open circle: hole; closed circle: electron.) A pair of hole and electron indicates an exciton.

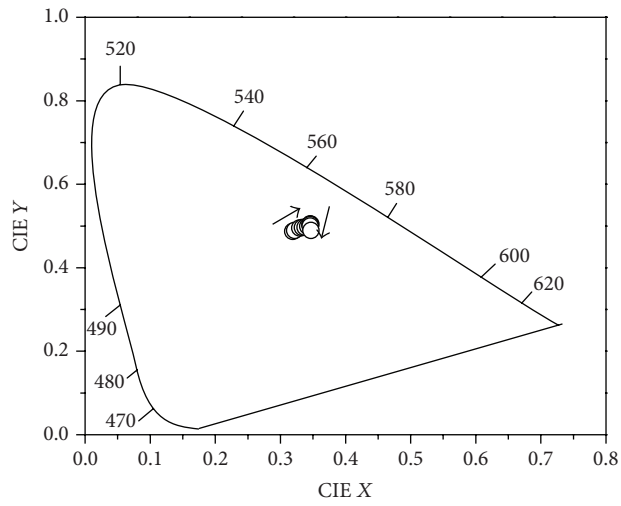

Figure 6: CIE coordinates of PFO/TiO_2 OLED devices when the applied voltage was increased from 18 to 29 V.

the interface between the Al cathode and the PFO/TiO_2 layer, which assisted electron injection [1].

As shown in Table 1, it can be seen that the device at 5 wt.% TiO_2 NPs exhibited significantly better optoelectronic properties compared to other devices. Despite similar roughness with pristine PFO device, the superior optoelectronic properties of this device suggest the importance of TiO_2 NPs in the nanocomposite system compared to roughness.

As TiO_2 NP contents increased, the devices continued to exhibit reduction in turn-on voltage, a direct consequence of increment in roughness [1]. Unfortunately, this reduction was at the expense of luminance and luminance efficiency. For example, at 15 wt.% TiO_2 NPs content, the luminance and luminance efficiency were dropped by 8% and 45%, respectively, compared to the same parameters for device with 5 wt.% TiO_2 NPs content. As the TiO_2 NPs content increased to 25 wt.%, the luminance was halved from the highest value while luminance efficiency was significantly inferior even if compared to pristine PFO. The huge reduction in both properties was contributed by the gigantic increment in surface roughness attributed to the presence of large amount of TiO_2 NPs.

A more dramatic reduction can be observed in device with 35 wt.% TiO_2 NPs content in which the presence of large protuberance, although produce similar roughness with 25 wt.% TiO_2 NPs, resulted in the material to lose its semiconducting behavior as demonstrated in Figure 1. Due to severe agglomeration, this nanocomposite behaved as matrix material which reduced the interface between PFO and TiO_2 NPs and hence significantly reduced charge transport. Similar observation has been reported by Madhave Rao and coworkers in a 2,3-dibutoxy-1,4-poly (phenylene vinylene) (DBPPV)/ZnO nanocomposite at high content of ZnO NRs [1]. Additional evidence of severe agglomeration in the PFO/ TiO_2 nanocomposites system has been demonstrated by FE-SEM images [11].

4. Conclusion

The solution blending method was successfully used to prepare PFO/TiO_2 nanocomposites, which were used as emissive layer in OLED devices. The optoelectronic properties of the devices were strongly influenced by the TiO_2 weight fraction. Based on the current work, the device with 5 wt.% of TiO_2 NPs exhibited the best performance contributed by optimum balance between holes and electrons recombination as well as good surface roughness. In contrast, the device with 35 wt.% displayed the worst performance attributed mainly to extremely high surface roughness and agglomeration. The red-shift of CIE coordinates, which related to maximum luminance, upon addition of TiO_2 NPs illustrating the extension of the recombination zone for holes and electrons in the OLED devices. The current work showed that carefully control TiO_2 NPs content in the starting composition is crucial to achieve optimum balance for excitons recombination

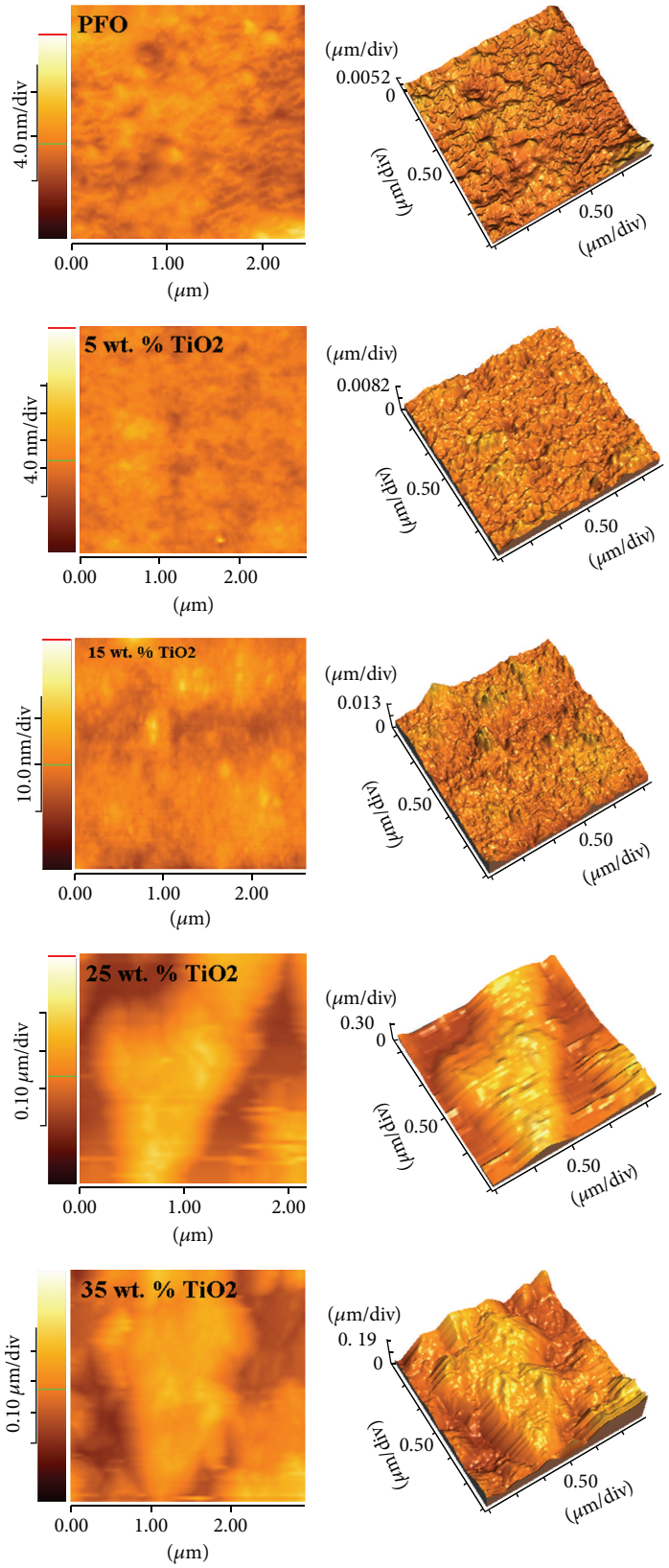

Figure 7: 2D and 3D SPM images of PFO and PFO/TiO_2 nanocomposites measured over an area of $2.5 \times 2.5\ \mu m^2$.

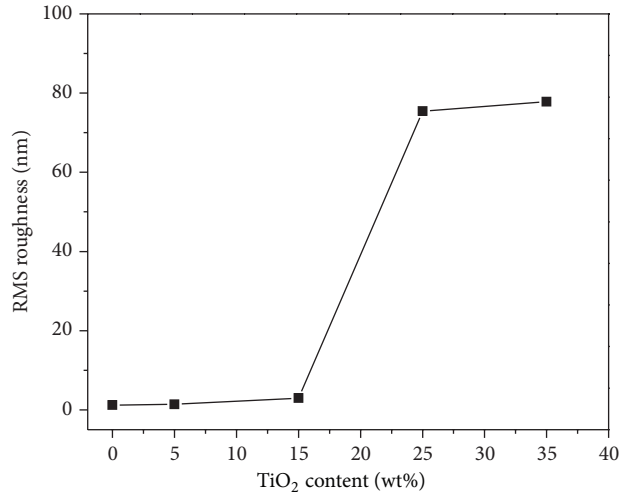

Figure 8: Root mean square (RMS) roughness for PFO/TiO_2 films as a function of TiO_2 NPs content.

and suitable for the surface roughness for better devices performance.

Acknowledgment

The authors would like to thank the Universiti Kebangsaan Malaysia (UKM) for providing excellent research facilities, under the Research University Grants DPP-2013-048 and DLP-2013-012.

References

[1] M. V. Madhava Rao, Y. K. Su, T. S. Huang, C.-H. Yeh, and M.-L. Tu, "Electroluminescent characteristics of DBPPV-ZnO nanocomposite polymer light emitting devices," *Nanoscale Research Letters*, vol. 4, no. 5, pp. 485–490, 2009.

[2] M. Willander, O. Nur, S. Zaman, A. Zainelabdin, N. Bano, and I. Hussain, "Zinc oxide nanorods/polymer hybrid heterojunctions for white light emitting diodes," *Journal of Physics D*, vol. 44, no. 22, Article ID 224017, 2011.

[3] M. Cocchi, J. Kalinowski, D. Virgili, and J. A. G. Williams, "Excimer-based red/near-infrared organic light-emitting diodes with very high quantum efficiency," *Applied Physics Letters*, vol. 92, no. 11, Article ID 113302, 2008.

[4] M. C. Suh, H. K. Chung, S.-Y. Kim, J. H. Kwon, and B. D. Chin, "Cathode diffusion and degradation mechanism of polymeric light emitting devices," *Chemical Physics Letters*, vol. 413, no. 1–3, pp. 205–209, 2005.

[5] H. Yang and P. H. Holloway, "Electroluminescence from hybrid conjugated polymer-Cds:Mn/ZnS core/shell nanocrystals devices," *Journal of Physical Chemistry B*, vol. 107, no. 36, pp. 9705–9710, 2003.

[6] M. J. Tommalieh and A. M. Zihlif, "Optical properties of polyimide/silica nanocomposite," *Physica B: Condensed Matter*, vol. 405, no. 23, pp. 4750–4754, 2010.

[7] A. Kongsinlark, G. L. Rempel, and P. Prasassarakich, "Synthesis of monodispersed polyisoprene-silica nanoparticles via differential microemulsion polymerization and mechanical properties of polyisoprene nanocomposite," *Chemical Engineering Journal*, vol. 193-194, pp. 215–226, 2012.

[8] J. Rozra, I. Saini, A. Sharma et al., "Cu nanoparticles induced structural, optical and electrical modification in PVA," *Materials Chemistry and Physics*, 2012.

[9] E. Dovgolevsky, S. Kirmayer, E. Lakin, Y. Yang, C. J. Brinker, and G. L. Frey, "Self-assembled conjugated polymer-surfactant-silica mesostructures and their integration into light-emitting diodes," *Journal of Materials Chemistry*, vol. 18, no. 4, pp. 423–436, 2008.

[10] A. Cirpan, L. Ding, and F. E. Karasz, "Optical and electroluminescent properties of polyfluorene copolymers and their blends," *Polymer*, vol. 46, no. 3, pp. 811–817, 2005.

[11] M. H. H. Jumali, B. A. Al-Asbahi, C. C. Yap, M. M. Salleh, and M. S. Alsalhi, "Optoelectronic property enhancement of conjugated polymer in poly (9,9′-di-n-octylfluorenyl-2.7-diyl)/titania nanocomposites," *Thin Solid Films*, vol. 524, pp. 257–262, 2012.

[12] M. Bajpai, R. Srivastava, M. N. Kamalasanan, R. S. Tiwari, and S. Chand, "Charge transport and microstructure in PFO:MEH-PPV polymer blend thin films," *Synthetic Metals*, vol. 160, no. 15-16, pp. 1740–1744, 2010.

[13] M. Skompska, "Hybrid conjugated polymer/semiconductor photovoltaic cells," *Synthetic Metals*, vol. 160, no. 1-2, pp. 1–15, 2010.

[14] A. C. Arango, S. A. Carter, and P. J. Brock, "Charge transfer in photovoltaics consisting of interpenetrating networks of conjugated polymer and TiO_2 nanoparticles," *Applied Physics Letters*, vol. 74, no. 12, pp. 1698–1700, 1999.

[15] A. M. Assaka, P. C. Rodrigues, A. R. M. De Oliveira et al., "Novel fluorine containing polyfluorenes with efficient blue electroluminescence," *Polymer*, vol. 45, no. 21, pp. 7071–7081, 2004.

[16] K. Sakamoto, K. Usami, Y. Uehara, and S. Ushioda, "Excellent uniaxial alignment of poly(9,9-dioctylfluorenyl-2,7-diyl) induced by photoaligned polyimide films," *Applied Physics Letters*, vol. 87, no. 21, Article ID 211910, 3 pages, 2005.

[17] B. Arredondo, B. Romero, A. Gutiérrez-Llorente et al., "On the electrical degradation and green band formation in α- and β-phase poly(9,9-dioctyfluorene) polymer light-emitting diodes," *Solid-State Electronics*, vol. 61, no. 1, pp. 46–52, 2011.

[18] Z. Chen and D. Ma, "Improved color purity and efficiency in polyfluorene-based light-emitting diodes," *Materials Science and Engineering B*, vol. 141, no. 1-2, pp. 71–75, 2007.

[19] X. Gong, P. K. Iyer, D. Moses, G. C. Bazan, A. J. Heeger, and S. S. Xiao, "Stabilized blue emission from polyfluorene-based light-emitting diodes: elimination of fluorenone defects," *Advanced Functional Materials*, vol. 13, no. 4, pp. 325–330, 2003.

[20] A. P. Kulkarni, C. J. Tonzola, A. Babel, and S. A. Jenekhe, "Electron transport materials for organic light-emitting diodes," *Chemistry of Materials*, vol. 16, no. 23, pp. 4556–4573, 2004.

[21] S. H. Kim, S. H. Park, and K. Lee, "Efficiency enhancement in polymer optoelectronic devices by introducing titanium suboxide layer," *Current Applied Physics*, vol. 10, no. 3, pp. S528–S531, 2010.

[22] C.-H. Hsiao, S.-W. Liu, C.-T. Chen, and J.-H. Lee, "Emitting layer thickness dependence of color stability in phosphorescent organic light-emitting devices," *Organic Electronics*, vol. 11, no. 9, pp. 1500–1506, 2010.

[23] R.-H. Lee and H.-H. Lai, "Enhancing electroluminescence performance of MEH-PPV based polymer light emitting device via blending with organosoluble polyhedral oligomeric silsesquioxanes," *European Polymer Journal*, vol. 43, no. 3, pp. 715–724, 2007.